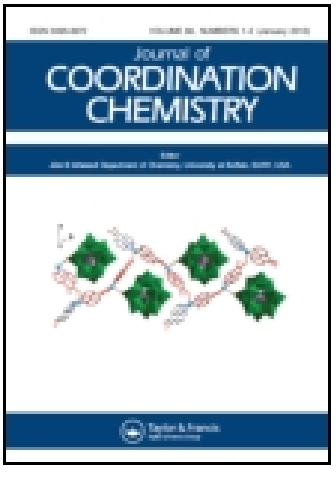

Journal of Coordination Chemistry
Publication details, including instructions for authors and subscription information:
http://www.tandfonline.com/loi/gcoo20

Syntheses, crystal structures, thermal behaviors, and sensitivities of new initiator compositions: rubidium salts of trinitrophenol and trinitroresorcinol

Zhi-Min Li[a], Tong-Lai Zhang[a], Hui-Sheng Huang[b], Jian-Guo Zhang[a], Li Yang[a], Zun-Ning Zhou[a] & Kai-Bei Yu[c]

[a] State Key Laboratory of Explosion Science and Technology, Beijing Institute of Technology, Beijing, PR China

[b] Chongqing Key Laboratory of Inorganic Special Functional Materials, College of Chemistry and Chemical Engineering, Yangtze Normal University, Chongqing, PR China

[c] Chengdu Branch, Chinese Academy of Sciences, Chengdu, PR China

Accepted author version posted online: 09 Jun 2014.Published online: 08 Jul 2014.

To cite this article: Zhi-Min Li, Tong-Lai Zhang, Hui-Sheng Huang, Jian-Guo Zhang, Li Yang, Zun-Ning Zhou & Kai-Bei Yu (2014) Syntheses, crystal structures, thermal behaviors, and sensitivities of new initiator compositions: rubidium salts of trinitrophenol and trinitroresorcinol, Journal of Coordination Chemistry, 67:11, 1923-1937, DOI: 10.1080/00958972.2014.932353

To link to this article: http://dx.doi.org/10.1080/00958972.2014.932353

Journal of Coordination Chemistry, 2014
Vol. 67, No. 11, 1923–1937, http://dx.doi.org/10.1080/00958972.2014.932353

Syntheses, crystal structures, thermal behaviors, and sensitivities of new initiator compositions: rubidium salts of trinitrophenol and trinitroresorcinol

ZHI-MIN LI†¶, TONG-LAI ZHANG*†, HUI-SHENG HUANG*‡, JIAN-GUO ZHANG†, LI YANG†, ZUN-NING ZHOU† and KAI-BEI YU§

†State Key Laboratory of Explosion Science and Technology, Beijing Institute of Technology, Beijing, PR China
‡Chongqing Key Laboratory of Inorganic Special Functional Materials, College of Chemistry and Chemical Engineering, Yangtze Normal University, Chongqing, PR China
§Chengdu Branch, Chinese Academy of Sciences, Chengdu, PR China

(*Received 19 January 2014; accepted 4 May 2014*)

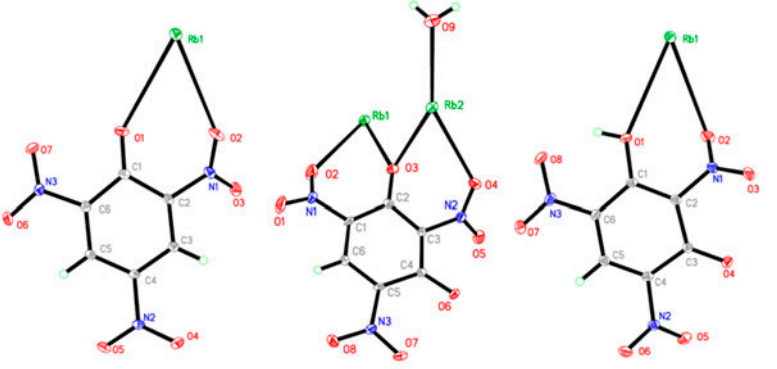

Three rubidium salts of trinitrophenol and trinitroresorcinol were obtained and characterized in this article. Thermal behaviors and sensitivities investigation confirmed them to be promising heat-resistant flame sensitive eco-friendly initiator composition.

Three new polymeric Rb(I) salts of trinitrophenol and trinitroresorcinol, rubidium trinitrophenol ($[RbTNP]_n$), bi-substituted rubidium salt of trinitroresorcinol ($[Rb_2TNR{\cdot}H_2O]_n$), and mono-substituted rubidium salt of trinitroresorcinol ($[RbHTNR]_n$) were synthesized and characterized by X-ray single-crystal diffraction, elemental analysis, and IR spectroscopy. The central Rb(I) cations are 10 or 11-coordinated by oxygens from nitro group, phenolic hydroxyl and coordinated water, and the multidentate ligands bridged different Rb(I) centers. Coordination bonds, electrostatic interaction, and intermolecular hydrogen bonds assemble the ions into 3-D polymeric network structures. Thermal decomposition behaviors of the compounds were studied by applying differential scanning

*Corresponding authors. Email: ztlbit@bit.edu.cn (T.-L. Zhang); h.s.huang@hotmail.com (H.-S. Huang)
¶Present address: Beijing Key Laboratory of Ionic Liquids Clean Process, Institute of Process Engineering, Chinese Academy of Sciences, Beijing, PR China.

calorimetry under various linear heating rates. Sensitivities measurements revealed that these compounds are sensitive to flame, insensitive to impact and friction stimulates. All properties show that the compounds are promising to be an eco-friendly initiating composition, especially $[RbTNP]_n$.

Keywords: Rubidium salts; Trinitrophenol; Trinitroresorcinol; Crystal structure; Properties

1. Introduction

Initiator composition as the primary energy to ignite a secondary explosive has been widely applied [1–3]. Lead trinitroresorcinol is one of the most famous initiator compositions and is widely used in military and civilian areas since it was identified in 1907 [4–7], due to its excellent properties, especially the sensitivity to flame. But, lead trinitroresorcinol is very sensitive to electrostatic discharge, which caused many terrible accidents. Deleterious environmental impacts and effects on human health have made replacement essential. Many works on energetic coordination compounds as the replacement of lead trinitroresorcinol have been accomplished [8–14].

Trinitro-substituted phenol compounds (2,4,6-trinitrophenol, HTNP; 2,4,6-trinitroresorcinol, H_2TNR; 2,4,6- trinitrophloroglucinol, H_3TNPG) are well-known explosives, and their metallic salts and complexes are promising ingredients of primary explosives and propellants [15–23]. To obtain eco-friendly initiator compositions, interests are focused on alkali salts of tri-nitro hydroxybenzenes. Potassium salt of trinitrophenol (KTNP) was studied by Shao *et al.* [24], then, Sheng *et al.* [19] investigated synthesis, properties, and applications, and confirmed it as an initiator composition. The structures and thermal decomposition mechanisms of di-substituted (K_2TNR) and mono-substituted (KHTNR) potassium salts of trinitroresorcinol were reported by Li *et al.* [25, 26]. Chen *et al.* investigated the structures and performances of mono-substituted (KH_2TNPG), di-substituted (K_2HTNPG), and tri-substituted (K_3TNPG) potassium salts of trinitrophloroglucinol and recommended them as components of clean initiating compositions and ignition [27, 28]. Energetic Rb salts have aroused attention in recent years. Chen *et al.* [29] reported the crystal structure and thermal behavior of mono-substituted rubidium salt of trinitrophloroglucinol (RbH_2TNPG). Klapötke *et al.* [30, 31] investigated the structures and energetic properties of rubidium salts of 5-(5-nitrotetrazole-2-ylmethyl)-tetrazolate and 5-nitrotetrazole. Luo *et al*. [32] investigated the synthesis and thermal behaviors of Rb salt of 1,1-diamino-2,2-dinitroethylene.

The present article focused on Rb salts of trinitrophenol and trinitroresorcinol. Three new energetic Rb salts were synthesized, the crystal structures were studied, and their thermal decomposition behaviors and sensitivities were determined to assess their potential application as energetic materials.

2. Experimental

2.1. *Materials and instruments*

All the reagents and solvents were of analytical grade and used without purification as commercially obtained. Elemental analyses (C, H, and N) were performed on the Elementar Vario MICROCUBE (Germeny) full-automatic trace element analyzer. IR spectra were recorded on a Bruker Equinox 55 infrared spectrometer (KBr pellets, Germany) from 4000 to 400 cm^{-1} with a resolution of 4 cm^{-1}. Thermal behaviors were investigated by

differential scanning calorimeter (DSC) (CDR-4, Shanghai Precision & Scientific Instrument Co., Ltd); about 0.5 mg sample was placed in aluminum pans in static air at various heating rates (5, 10, 15, and 20 K min^{-1}) from room temperature to 873 K.

2.2. *Synthesis of $[RbTNP]_n$*

5.8 g (0.025 M) HTNP and 0.5 g (0.0125 M) MgO were put into 100 mL deionized water with strong stirring at 343 K and a few minutes later, clear aqueous solution of $Mg(TNP)_2$ was obtained. $RbNO_3$ aqueous solution (3.7 g (0.025 M) $RbNO_3$ dissolved in 40 mL deionized water) was poured into the $Mg(TNP)_2$ solution at 343 K. The mixture was stirred at this temperature for 10 min, then cooled to room temperature rapidly, and filtered. The product was obtained and washed with ethanol twice, and dried in a water bath oven at 323 K for 6 h, yield 86%. Anal. Calcd (%) for $C_6H_2N_3O_7Rb$: C, 22.94; H, 0.64; N, 13.38. Found: C, 23.12; H, 0.66; N, 13.25. IR (KBr) ν (cm^{-1}): 3028, 1669, 1541, 1395, 1283, 941, 874, 763. The synthetic route of $[RbTNP]_n$ is shown in scheme 1.

2.3. *Synthesis of $[Rb_2TNR{\cdot}H2O]_n$*

6.1 g (0.025 M) H_2TNR and 1 g (0.025 M) MgO were put into 100 mL deionized water with strong stirring at 343 K and a few minutes later, clear aqueous solution of MgTNR was obtained. $RbNO_3$ aqueous solution (7.4 g (0.05 M) $RbNO_3$ dissolved in 80 mL deionized water) was poured into the MgTNR solution at 343 K. The mixture was stirred at this temperature for 10 min, then cooled to room temperature rapidly and filtered. The product was obtained and washed with ethanol twice, and dried in a water bath oven at 323 K for 6 h, yield 72%. Anal. Calcd (%) for $C_6H_3N_3O_9Rb_2$: C, 16.67; H, 0.69; N, 9.72. Found: C, 16.85; H, 0.74; N, 9.57. IR (KBr) ν (cm^{-1}): 3428, 2913, 1643, 1495, 1382, 1311, 895, 723. The synthetic route of $[Rb_2TNR{\cdot}H_2O]_n$ is shown in scheme 2.

2.4. *Synthesis of $[RbHTNR]_n$*

6.1 g (0.025 M) H_2TNR and 1 g (0.025 M) MgO were put into 100 mL deionized water with strong stirring at 343 K and a few minutes later, clear aqueous solution of MgTNR was

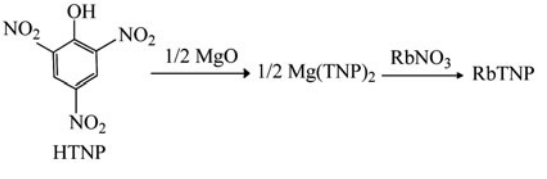

Scheme 1. The synthetic route of $[RbTNP]_n$.

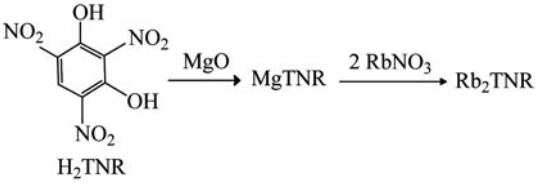

Scheme 2. The synthetic route of $[Rb_2TNR{\cdot}H_2O]_n$.

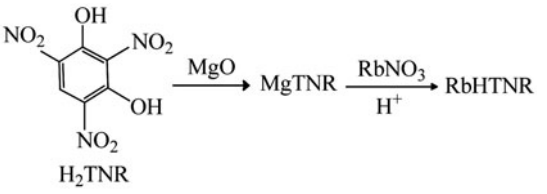

Scheme 3. The synthetic route of $[RbHTNR]_n$.

obtained. The pH of the solution was adjusted to 3–4 by adding dilute nitric acid. $RbNO_3$ aqueous solution (3.7 g (0.025 M) $RbNO_3$ dissolved in 40 mL deionized water) was poured into the MgTNR solution at 343 K. The mixture was stirred at this temperature for 10 min, then cooled to room temperature rapidly and filtered. The product was obtained and washed with ethanol twice, and dried in a water bath oven at 323 K for 6 h, yield 78%. Anal. Calcd (%) for $C_6H_2N_3O_8Rb$: C, 21.85; H, 0.61; N, 12.74. Found: C, 21.78; H, 0.69; N, 12.91. IR (KBr) ν (cm^{-1}): 3476, 2932, 1651, 1478, 1409, 1288, 916, 843. The synthetic route of $[RbHTNR]_n$ is shown in scheme 3.

2.5. *X-ray crystallography*

The X-ray diffraction data collections were performed on a Rigaku AFC-10/Saturn 724^+ CCD diffractometer with graphite-monochromated Mo K_α radiation ($\lambda = 0.71073$ Å) using the multi-scan technique. The structures were solved by direct methods using SHELXS-97 and refined by full-matrix least-squares procedures on F^2 with SHELXL-97 [33–35]. All non-hydrogen atoms were obtained from the difference Fourier map and subjected to anisotropic refinement by full-matrix least squares on F^2. Hydrogens were obtained geometrically and treated as riding on the parent atoms or were constrained in the locations during refinements. Detailed information of crystallographic data collection and structures refinement is summarized in table 1.

2.6. *Sensitivity measurements*

Impact sensitivity (50% firing height, H_{50}) was measured by Bruceton staircase method, 10 kg drop hammer, and 50 mg sample mass. Friction sensitivity (probability of explosion, P) was measured by 1.5 kg pendulum hammer fixed on 66° tilt angle, 2.45 MPa gage pressure, and 20 mg sample mass. For flame sensitivity (50% firing height, H_{50}), 20 mg sample was compacted into a copper cap under 58.8 MPa and was ignited with a standard black powder pellet. The 5 s delay explosive temperature (T_5) was measured with a copper detonator shell, wood's alloy bath, and 30 mg sample mass.

3. Results and discussion

3.1. *Crystal structures*

The crystals of $[RbTNP]_n$ and $[RbHTNR]_n$ belong to the monoclinic system, *P2(1)/c* and *P2(1)/n* space groups, respectively, whereas $[Rb_2TNR{\cdot}H_2O]_n$ belongs to the triclinic system,

Table 1. Crystallographic data and structure refinement details for $[RbTNP]_n$, $[Rb_2TNR{\cdot}H_2O]_n$, and $[RbHTNR]_n$.

Empirical formula	$C_6H_2N_3O_7Rb$	$C_6H_3N_3O_9Rb_2$	$C_6H_2N_3O_8Rb$
Formula weight (g M^{-1})	313.84	432.05	329.58
Temperature (K)	143(2)	296(2)	143(2)
Crystal dim. (mm)	0.43 × 0.20 × 0.13	0.36 × 0.26 × 0.12	0.20 × 0.14 × 0.11
Crystal system	Monoclinic	Triclinic	Monoclinic
Space group	*P2(1)/c*	*P-1*	*P2(1)/n*
a (Å)	10.529(4)	7.115(1)	4.4991(11)
b (Å)	4.5347(14)	9.677(2)	10.850(3)
c (Å)	19.061(7)	10.053(1)	19.489(5)
α (°)	90.00	115.29(1)	90.00
β (°)	101.708(4)	108.32(1)	91.549(3)
γ (°)	90.00	95.86(1)	90.00
V/Å^3	891.1(5)	571.02(18)	951.0(4)
ρ (g cm^{-3})	2.337	2.512	2.302
Z	11	2	4
μ (mm^{-1})	5.591	8.62	5.25
F(0 0 0)	608	412	640
θ ranges (°)	2.4–31.5	6.5–18.5	2.1–31.5
Limiting indices	$-15 \le h \le 15$	$0 \le h \le 8$	$-6 \le h \le 6$
	$-5 \le k \le 6$	$-10 \le k \le 10$	$-15 \le k \le 15$
	$-25 \le l \le 28$	$-11 \le l \le 11$	$-26 \le l \le 28$
Reflections collected	10,586	2275	12,253
Independent reflections (R_{int})	2869 (0.038)	1953 (0.022)	3129 (0.046)
Data/restraints/parameters	2869/0/155	1953/3/190	3129/1/167
Goodness-of-fit on F^2	1.001	0.897	1.004
Final R_1, wR_2 $[I > 2\sigma(I)]$[a]	0.0298, 0.0648	0.0287, 0.0491	0.0382, 0.0973
R_1, wR_2 indices (all data)[a]	0.0375, 0.0679	0.0508, 0.0506	0.0502, 0.1026
Largest diff. peak and hole (e Å^{-3})	0.53 and –0.89	0.42 and –0.60	1.26 and –0.79

[a]$w = 1/[\sigma^2(F_o^2) + (0.0335P)^2 + 0.360P]$ for $[RbTNP]_n$, $w = 1/[\sigma^2(F_o^2) + (0.0202P)^2]$ for $[Rb_2TNR{\cdot}H_2O]_n$, $w = 1/[\sigma^2(F_o^2) + (0.0516P)^2 + 0.9160P]$ for $[RbHTNR]_n$, where $P = (F_o^2 + 2F_c^2)/3$.

P-1 space group. The crystal density of $[RbTNP]_n$, $[Rb_2TNR{\cdot}H_2O]_n$, and $[RbHTNR]_n$ are 2.337, 2.512, and 2.302 g cm^{-3}, respectively. The molecular unit and labeling scheme of $[RbTNP]_n$, $[Rb_2TNR{\cdot}H_2O]_n$, and $[RbHTNR]_n$ are shown in figure 1. The asymmetric unit of $[RbTNP]_n$ is comprised of one Rb(I) and one TNP^-, $[Rb_2TNR{\cdot}H_2O]_n$ is comprised of two Rb(I) centers, one TNR^{2-}, and one coordinated H_2O, and $[RbHTNR]_n$ is comprised of one Rb(I) and one $HTNR^-$. Selected bond lengths and angles for $[RbTNP]_n$, $[Rb_2TNR{\cdot}H_2O]_n$, and $[RbHTNR]_n$ are given in table 2. The hydrogen bond parameters are summarized in table 3.

Figure 2 shows the coordination environment of TNP^- ligand and Rb(I), as well as the packing diagram of $[RbTNP]_n$ viewed along the *b*-axis. In $[RbTNP]_n$, the central Rb(I) is coordinated by 11 oxygens from seven different TNP^- ligands. The bond lengths of Rb–O are 2.89–3.38 Å, bigger than K–O lengths (2.74–2.92 Å) in KTNP [24] and shorter than Cs–O lengths (3.03–3.54 Å) in CsTNP [36]. This can be attributed to the radius of K(I), Rb (I), and Cs(I). As shown in figure 2(a), TNP^- is coordinated with seven different Rb(I) centers. The 3-D polymeric network was formed by multidentate TNP^- ligands bridging adjacent Rb(I) ions, as shown in figure 1(c).

Figure 3 shows the coordination environment of TNR^{2-} and two Rb(I) centers, as well as the packing diagram of $[Rb_2TNR{\cdot}H_2O]_n$ viewed along the *a*-axis. Both Rb(I) centers are coordinated by 10 oxygens, coordinated to Rb1 from seven different TNR^{2-} ligands, and for Rb2 from six different TNR^{2-} ligands. Rb–O bond lengths are 2.76–3.42 Å, also between the K–O lengths (2.64–3.19 Å) of K_2TNR [26] and Cs–O lengths (3.03–3.58 Å) of Cs_2TNR [37]. TNR^{2-} coordinated with 12 different Rb(I) centers, including six Rb1 and six Rb2. H_2O bridged one Rb1 and one Rb2. The multidentate TNR^{2-} ligands and H_2O molecules joined various Rb(I) centers to form a 3-D polymeric structure. Furthermore, two kind of hydrogen bonds were formed between O9 (water) and O5 (nitro group) and O6 (phenolic hydroxyl), O9–H9A$\cdots$O5^{xiii} and O9–H9B$\cdots$EO6^{ix}.

Figure 4 shows the coordination environment of $HTNR^-$ ligand and Rb(I), as well as the packing diagram of $[RbHTNR]_n$ viewed along the *a*-axis. In $[RbHTNR]_n$, the central Rb(I) is coordinated by 10 oxygens from seven different $HTNR^-$ ligands. The bond lengths of

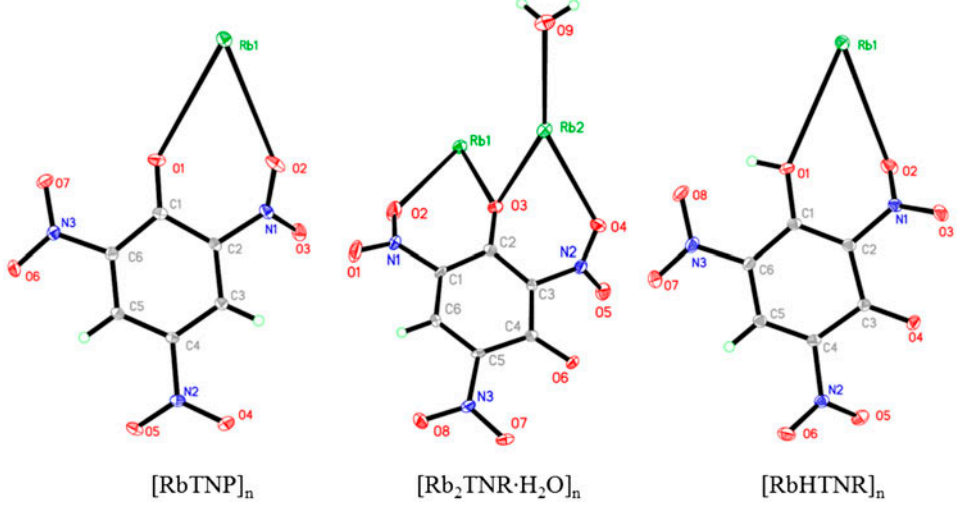

Figure 1. Molecular unit and labeling scheme of $[RbTNP]_n$, $[Rb_2TNR{\cdot}H_2O]_n$, and $[RbHTNR]_n$.

Table 2. Selected bond lengths (Å) and angles (°) for $[RbTNP]_n$, $[Rb_2TNR{\cdot}H_2O]_n$, and $[RbHTNR]_n$.

$[RbTNP]_n$							
Rb1–O7^{i}	2.8663 (17)	Rb1–O6^{vi}	3.3135 (17)	C1–O1–Rb1^{vii}	108.22 (13)	N3–O7–Rb1^{vii}	114.36 (12)
Rb1–O1^{ii}	2.9209 (17)	Rb1–O4^{v}	3.3792 (18)	C1–O1–Rb1	144.92 (14)	N3–O7–Rb1^{ix}	102.27 (12)
Rb1–O3^{iii}	3.0192 (17)	O1–C1	1.243 (2)	N1–O2–Rb1	143.89 (13)	Rb1^{vii}–O1–Rb1	96.58 (5)
Rb1–O3^{iv}	3.0270 (18)	O2–N1	1.229 (2)	N1–O3–Rb1^{iii}	118.82 (13)	Rb1^{iii}–O3–Rb1^{iv}	97.18 (5)
Rb1–O2	3.0537 (18)	O3–N1	1.235 (2)	N1–O3–Rb1^{iv}	139.64 (13)	Rb1^{x}–O7–Rb1^{vii}	109.98 (5)
Rb1–O7^{ii}	3.0586 (18)	O4–N2	1.235 (2)	N2–O4–Rb1^{viii}	89.23 (11)	Rb1^{x}–O7–Rb1^{ix}	96.82 (5)
Rb1–O1	3.1501 (16)	O5–N2	1.234 (2)	N2–O5–Rb1^{viii}	99.87 (11)	Rb1^{vii}–O7–Rb1^{ix}	101.92 (5)
Rb1–O5^{v}	3.1577 (18)	O6–N3	1.236 (2)	N3–O6–Rb1^{ix}	96.17 (11)		
Rb1–O7^{vi}	3.1901 (18)	O7–N3	1.238 (2)	N3–O7–Rb1^{x}	126.15 (13)		
$[Rb_2TNR{\cdot}H_2O]_n$							
Rb1–O3	2.759 (3)	Rb2–O5^{v}	3.041 (3)	C4–O6–Rb1^{x}	148.1 (3)	N3–O8–Rb2^{viii}	106.6 (2)
Rb1–O6^{i}	2.783 (3)	Rb2–O7^{viii}	3.359 (3)	N1–O1–Rb1^{iv}	111.0 (3)	Rb2^{iv}–O1–Rb1^{iv}	84.72 (9)
Rb1–O1^{iv}	3.113 (4)	Rb2–O8^{vii}	2.868 (3)	N1–O1–Rb2^{iv}	103.9 (3)	Rb1–O2–Rb2^{iv}	120.20 (12)
Rb1–O2	3.066 (3)	Rb2–O8^{viii}	3.073 (3)	N1–O2–Rb1	141.7 (3)	Rb1–O2–Rb1^{vi}	80.02 (9)
Rb1–O2^{vi}	3.318 (4)	Rb2–O9	2.856 (4)	N1–O2–Rb1^{vi}	126.9 (3)	Rb2^{iv}–O2–Rb1^{vi}	74.50 (7)
Rb1–O4^{v}	3.167 (3)	O3–C2	1.247 (5)	N1–O2–Rb2^{iv}	95.2 (2)	Rb1–O3–Rb2	96.21 (9)
Rb1–O5^{v}	3.191 (3)	O6–C4	1.256 (5)	N2–O4–Rb1^{v}	97.7 (3)	Rb2–O4–Rb1^{v}	130.87 (11)
Rb1–O7^{i}	2.923 (3)	O1–N1	1.229 (4)	N2–O4–Rb2	130.9 (3)	Rb2–O4–Rb2^{ix}	80.93 (9)
Rb1–O7^{iii}	3.098 (4)	O2–N1	1.229 (5)	N2–O4–Rb2^{ix}	126.6 (3)	Rb1^{v}–O4–Rb2^{ix}	73.43 (7)
Rb1–O9^{ii}	3.039 (4)	O4–N2	1.243 (5)	N2–O5–Rb1^{v}	96.8 (2)	Rb2^{v}–O5–Rb1^{v}	83.08 (7)
Rb2–O3	2.795 (3)	O5–N2	1.232 (5)	N2–O5–Rb2^{v}	119.1 (3)	Rb1^{x}–O7–Rb1^{iii}	86.01 (9)
Rb2–O1^{iv}	3.021 (3)	O7–N3	1.238 (4)	N3–O7–Rb1^{x}	147.2 (3)	Rb1^{x}–O7–Rb2^{viii}	119.34 (11)
Rb2–O2^{iv}	3.194 (3)	O8–N3	1.238 (4)	N3–O7–Rb1^{iii}	112.5 (3)	Rb1^{iii}–O7–Rb2^{viii}	75.14 (7)
Rb2–O4	2.946 (4)	C2–O3–Rb1	143.9 (3)	N3–O7–Rb2^{viii}	92.3 (2)	Rb2^{xi}–O8–Rb2^{viii}	88.46 (8)
Rb2–O4^{ix}	3.419 (4)	C2–O3–Rb2	117.4 (3)	N3–O8–Rb2^{xi}	165.0 (3)	Rb2–O9–Rb1^{xii}	83.88 (9)
$[RbHTNR]_n$							
Rb1–O4^{i}	2.846 (2)	Rb1–O8^{vi}	3.251 (2)	O7–N3	1.231 (3)	N2–O5–Rb1^{viii}	138.39 (19)
Rb1–O6^{ii}	2.906 (2)	Rb1–O1	3.287 (2)	O8–N3	1.257 (3)	N2–O6–Rb1^{ix}	135.08 (19)
Rb1–O2^{iii}	2.924 (2)	O1–C1	1.330 (3)	C1–O1–Rb1	147.84 (19)	N2–O6–Rb1^{x}	113.55 (18)
Rb1–O3^{iv}	2.952 (2)	O4–C3	1.237 (3)	C3–O4–Rb1^{viii}	145.63 (19)	N3–O8–Rb1^{iv}	112.33 (18)
Rb1–O4^{iv}	3.043 (2)	O2–N1	1.233 (3)	C3–O4–Rb1^{vi}	110.30 (18)	Rb1^{vii}–O2–Rb1	93.93 (6)
Rb1–O5^{i}	3.065 (3)	O3–N1	1.230 (3)	N1–O2–Rb1^{vii}	133.69 (19)	Rb1^{viii}–O4–Rb1^{vi}	99.59 (7)
Rb1–O6^{v}	3.084 (2)	O5–N2	1.227 (4)	N1–O2–Rb1	125.90 (19)	Rb1^{ix}–O6–Rb1^{x}	97.32 (6)
Rb1–O2	3.225 (3)	O6–N2	1.237 (3)	N1–O3–Rb1^{vi}	134.55 (18)		

Note: Symmetry codes: $[RbTNP]_n$: (i) $-x+1, y+1/2, -z+3/2$; (ii) $x, y+1, z$; (iii) $-x+1, -y+3, -z+1$; (iv) $-x+1, -y+2, -z+1$; (v) $x-1, y+1, z$; (vi) $-x+1, y+3/2, -z+3/2$; (vii) $x, y-1, z$; (viii) $x+1, y-1, z$; (ix) $-x+1, y-3/2, -z+3/2$; (x) $-x+1, y-1/2, -z+3/2$. $[Rb_2TNR{\cdot}H_2O]_n$: (i) $x, y, z-1$; (ii) $x+1, y, z$; (iii) $-x+2, -y+1, -z+1$; (iv) $-x+1, -y+1, -z$; (v) $-x+2, -y+2, -z+1$; (vi) $-x+2, -y+1, -z$; (vii) $x, y+1, z$; (viii) $-x+1, -y+1, -z+1$; (ix) $-x+1, -y+2, -z+1$; (x) $x, y, z+1$; (xi) $x, y-1, z$; (xii) $x-1, y, z$. $[RbHTNR]_n$: (i) $-x+1/2, y+1/2, -z+1/2$; (ii) $x+1/2, -y+3/2, z-1/2$; (iii) $x+1, y, z$; (iv) $-x+3/2, y+1/2, -z+1/2$; (v) $x+3/2, -y+3/2, z-1/2$; (vi) $-x+3/2, y-1/2, -z+1/2$; (vii) $x-1, y, z$; (viii) $-x+1/2, y-1/2, -z+1/2$; (ix) $x-1/2, -y+3/2, z+1/2$; (x) $x-3/2, -y+3/2, z+1/2$.

Table 3. Hydrogen bond lengths (Å) and bond angles (°) for $[Rb_2TNR{\cdot}H_2O]_n$ and $[RbHTNR]_n$.

D–H···A	D–H(Å)	H···A (Å)	D–A (Å)	D–H···A (°)
$[Rb_2TNR{\cdot}H_2O]_n$				
O9–H9A···O5^{xiii}	0.82(2)	2.39(2)	3.159(6)	158(4)
O9–H9B···O6^{ix}	0.82(5)	2.10(6)	2.921(6)	173(8)
$[RbHTNR]_n$				
O1–H10···O8	0.84(2)	1.85(3)	2.570(3)	144(3)
O1–H10···N3	0.84(2)	2.45(4)	2.895(4)	114(3)
O1–H10···O3^{iv}	0.84(2)	2.21(4)	2.710(3)	119(3)

Note: Symmetry codes: $[Rb_2TNR{\cdot}H_2O]_n$: (xiii) $x-1, y, z-1$; (ix) $-x+1, -y+2, -z+1$. $[RbHTNR]_n$: (iv) $-x+3/2, y+1/2, -z+1/2$.

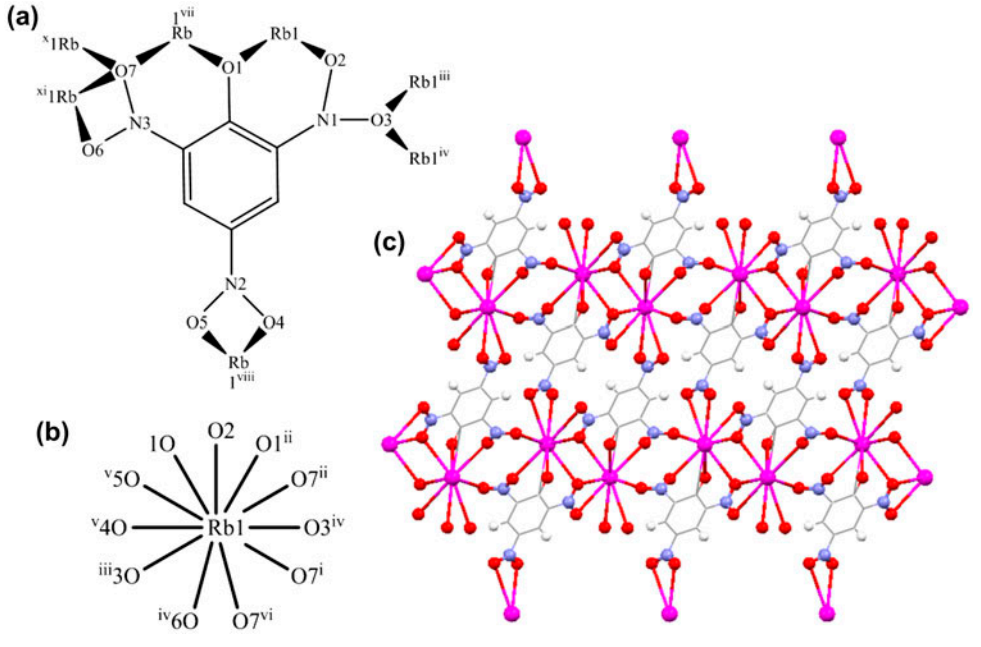

Figure 2. Coordination environment of (a) TNP^- and (b) Rb^+ center, (c) the packing diagram of $[RbTNP]_n$ viewed along the *b*-axis.

Rb–O are 2.85–3.29 Å, similar to mono-substituted rubidium salt of trinitrophloroglucinol (RbH_2TNPG, 2.94–3.22 Å) [29], also between the K–O lengths (2.77–2.92 Å) of KHTNR [35] and Cs–O lengths (3.00–3.76 Å) of CsHTNR [38]. $HTNR^-$ coordinated with seven different Rb(I) centers. The multidentate $HTNR^-$ ligands joined various Rb(I) centers to form a stable 3-D polymeric structure. Due to the un-substituted H atom from phenolic hydroxyl, three kinds of hydrogen bonds were formed between O1 (phenolic hydroxyl) and O8 (nitro group), O3 (nitro group) and N3 (nitro group): O1–H10···O8, O1–H10···O3^{iv} and O1–H10···N3. The hydrogen bonds make an important contribution to the stability of the compound.

3.2. *Thermal behaviors*

DSC was applied to assess the thermal decomposition behaviors of the compounds. Figure 5 shows the DSC curves of $[RbTNP]_n$, $[Rb_2TNR{\cdot}H_2O]_n$, and $[RbHTNR]_n$ at a heating rate of

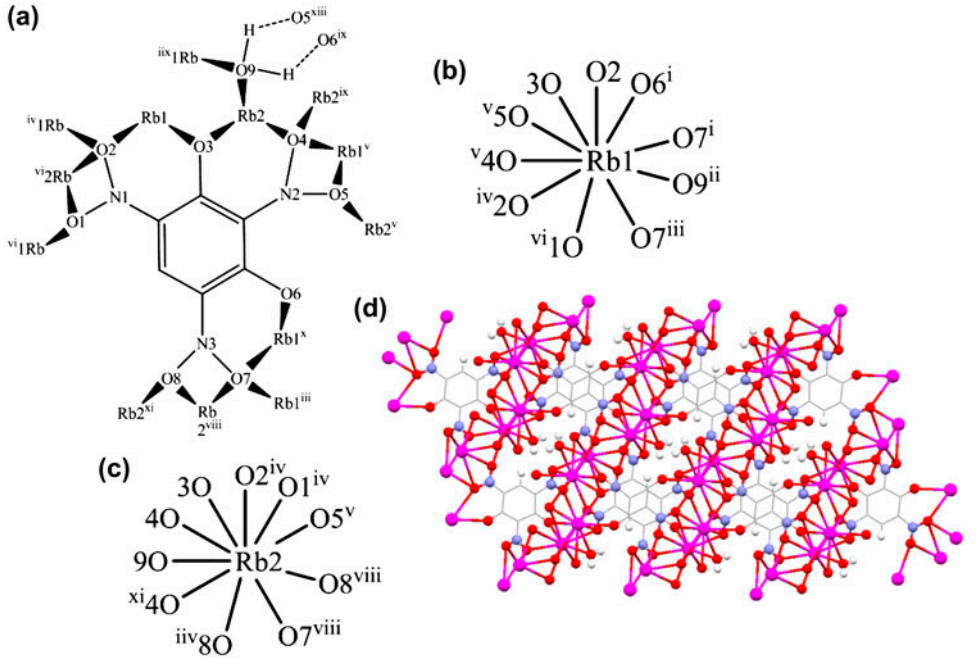

Figure 3. Coordination environment of (a) TNR^{2-} and (b), (c) Rb^{+} center, (d) the packing diagram of $[Rb_2TNR{\cdot}H_2O]_n$ viewed along the *a*-axis.

10 K min^{-1}. The peak temperatures (T_p) of the exothermic process of the studied compounds at heating rates of 5, 10, 15, and 20 K min^{-1} are listed in table 4.

Kissinger's [39] (equation (1)) and Ozawa's [40] (equation (2)) methods were used to determine the apparent activation energy and the pre-exponential factor of the exothermic process from the multiple non-isothermal peak temperatures,

$$\frac{d\ln(\beta/T_p^2)}{d(1/T_p)} = -\frac{E_a}{R} \tag{1}$$

$$\lg\beta + \frac{0.4567E_a}{RT_p} = C \tag{2}$$

where T_p is the peak temperature, K; R is the gas constant, 8.314 J M^{-1} K^{-1}; β is the linear heating rate, K min^{-1}; and C is a constant. The obtained apparent activation energy E_K and E_O, pre-exponential factor A_K, and linear correlation coefficient R_K and R_O of the exothermic decomposition process are shown in table 4; subscripts K and O denoted calculation results by Kissinger's method and Ozawa's method, respectively.

In figure 5, sharp exothermic peaks were found in the DSC curves of $[RbTNP]_n$, $[Rb_2TNR{\cdot}H_2O]_n$, and $[RbHTNR]_n$ at 587–621 K, 489–556 K, and 495–522 K, respectively. Furthermore, a small endothermic peak from 380 to 402 K was observed in the DSC curve of $[Rb_2TNR{\cdot}H_2O]_n$ due to the presence of coordinated water.

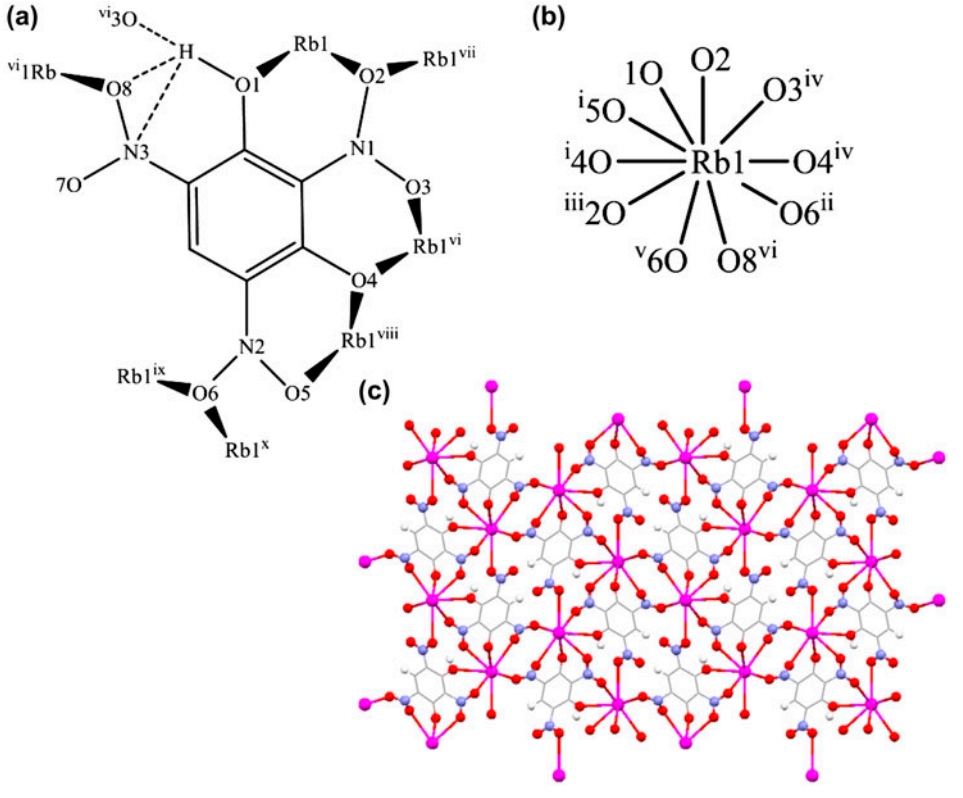

Figure 4. Coordination environment of (a) $HTNR^-$ and (b) Rb^+ center, (c) the packing diagram of $[RbHTNR]_n$ viewed along the *a*-axis.

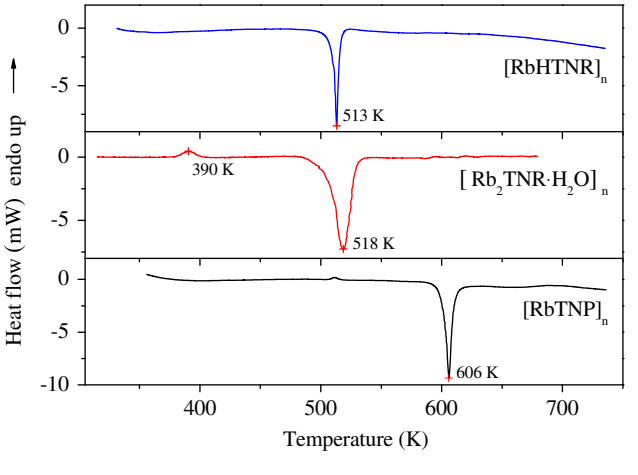

Figure 5. DSC curves of $[RbTNP]_n$, $[Rb_2TNR{\cdot}H_2O]_n$, and $[RbHTNR]_n$.

Table 4. The corresponding parameters of thermal behaviors for $[RbTNP]_n$, $[Rb_2TNR{\cdot}H_2O]_n$, and $[RbHTNR]_n$.

Compounds	$[RbTNP]_n$	$[Rb_2TNR{\cdot}H_2O]_n$	$[RbHTNR]_n$
T_p (K, $\beta = 5/10/15/20$ K min^{-1})	601/606/610/614	516/518/522/528	505/513/519/526
E_K (kJ M^{-1})/ln(A_K(s^{-1}))/R_K	318.5/25.65/–0.9899	227.4/21.06/–0.9107	138.6/12.10/–0.9871
E_O (kJ M^{-1})/R_O	312.5/–0.9905	224.5/–0.9164	139.9/–0.9886
T_{P0} (K)	596	516	497
T_{bP} (K)	606	526	513
$\triangle S^{\neq}$ (J M^{-1} K^{-1})	–13.29	–12.09	–11.78
$\triangle H^{\neq}$ (kJ M^{-1})	153.24	153.91	154.07
$\triangle G^{\neq}$ (kJ M^{-1})	161.16	160.15	159.92

The peak temperature of the exothermic process of $[RbTNP]_n$ at a heating rate of 10 K min^{-1} is 606 K, higher than that of $[Rb_2TNR{\cdot}H_2O]_n$ (518 K) and $[RbHTNR]_n$ (513 K). KTNP and K_2TNR are more stable than the corresponding rubidium salts, with the peak temperature of 612 and 592 K [19, 41]. Wang *et al.* [28] confirmed the acidic potassium salts of trinitrophloroglucinol (H_3TNPG) are thermally more sensitive than normal salt; thermal decomposition peak temperature of KH_2TNPG, K_2HTNPG, and K_3TNPG are 462, 533, and 568, respectively. The peak temperature of the intense exothermic process of RbH_2TNPG is 480 K [29], lower than that of $[RbHTNR]_n$. The sensitivity for both potassium and rubidium salts of nitro-phenol are trinitrophenol < trinitroresorcinol < trinitrophloroglucinol, ascribed to the active nitro group. The structure of normal salt of trinitroresorcinol is closer than that of acidic salt and Rb–O coordinate bonds are stronger than H-bonds, resulting in $[Rb_2TNR{\cdot}H_2O]_n$ being more stable than $[RbHTNR]_n$. The calculated results using Kissinger's and Ozawa's methods are similar and in the normal range of kinetic parameters for thermal decomposition of solid materials [42]. Using the values of apparent activation energy (the average of E_K and E_O) and pre-exponential constant, the Arrhenius equation of the exothermic process of $[RbTNP]_n$, $[Rb_2TNR{\cdot}H_2O]_n$, and $[RbHTNR]_n$ can be expressed as follows:

$$\ln k = 25.65 - 315.5 \times 10^3/RT,$$

$$\ln k = 21.06 - 226.0 \times 103/RT,$$

$$\ln k = 12.10 - 139.3 \times 103/RT.$$

The values of the peak temperature of the exothermic process corresponding to $\beta \to 0$ (T_{p0}) of $[RbTNP]_n$, $[Rb_2TNR{\cdot}H_2O]_n$, and $[RbHTNR]_n$ obtained according to equation (3) [43] are 596, 516, and 497 K, respectively, where b and c are coefficients. The corresponding critical temperature of thermal explosion (T_{bp}) obtained from following equation (4) [44, 45] of $[RbTNP]_n$, $[Rb_2TNR{\cdot}H_2O]_n$, and $[RbHTNR]_n$ are 606, 526, and 513 K, respectively. The values of T_{p0} and T_{bp} also confirmed the order of thermal stability of the title compounds as:

$$[RbTNP]_n > [Rb_2TNR \cdot H_2O]_n > [RbHTNR]_n$$

$$T_{pi} = T_{p0} + b\beta_i + c\beta_i^2 \tag{3}$$

$$T_{bp} = \frac{E_O - \sqrt{{E_O}^2 - 4E_O R T_{p0}}}{2R} \tag{4}$$

The entropy of activation ($\Delta S^{\neq}$), enthalpy of activation ($\Delta H^{\neq}$), and free energy of activation ($\Delta G^{\neq}$) of the exothermic decomposition process of the compounds corresponding to $T = T_{p0}$, $E_a = E_K$, and $A = A_K$ obtained by equations (5)–(7) [44, 45] are listed in table 4. The positive values of $\Delta G^{\neq}$ indicate that the exothermic decomposition reaction of the studied initiator compounds must proceed under the heating condition, and $[RbHTNR]_n$ is easier to decompose than $[Rb_2TNR{\cdot}H_2O]_n$ and $[RbTNP]_n$,

Table 5. The sensitivities of $[RbTNP]_n$, $[Rb_2TNR{\cdot}H_2O]_n$, and $[RbHTNR]_n$.

Compounds	$[RbTNP]_n$	$[Rb_2TNR{\cdot}H_2O]_n$	$[RbHTNR]_n$	KTNP [12]	K_2TNR [34]	PbTNR [7]
T_5 (K)	641	556	542	664	645	596
$H_{50}(F)$ (cm)	50	39	36	38	12	47
P (%)	no fire	no fire	no fire	2	–	68
$H_{50}(I)$ (cm)	no fire	no fire	no fire	28	–	12

Note: T_5: 5 s delay explosion temperature; $H_{50}(F)$: 50% firing height for flame; P: probability of fire from friction; $H_{50}(I)$: 50% firing height for impact.

$$A = \frac{k_B T}{h} e^{\Delta S^{\neq}/R} \tag{5}$$

$$\Delta H^{\neq} = E_a - RT \tag{6}$$

$$\Delta G^{\neq} = \Delta H^{\neq} - T\Delta S^{\neq} \tag{7}$$

where k_B is the Boltzmann constant (1.3807×10^{-23} J K^{-1}) and h is the Plank constant (6.626×10^{-34} J s^{-1}).

3.3. *Sensitivities*

The 5s delay explosive temperature, flame, impact, and friction sensitivities of $[RbTNP]_n$, $[Rb_2TNR{\cdot}H_2O]_n$, and $[RbHTNR]_n$ were determined and the results contrasted with the potassium and lead salts (table 5). All the studied compounds are sensitive to heat and flame stimulus, but not fire to impact and friction under the testing conditions. The 50% firing thresholds toward flame of $[RbTNP]_n$ is 50 cm, higher than lead trinitroresorcinol (PbTNR, 47 cm) [7]. $[Rb_2TNR{\cdot}H_2O]_n$ and $[RbHTNR]_n$ are also sensitive to flame as KTNP [19], with the $H_{50}(F)$ of 39, 36, and 38 cm, respectively. The 5 s delay explosive temperature of $[RbTNP]_n$ is 641 K, higher than that of $[Rb_2TNR{\cdot}H_2O]_n$ (556 K), $[RbHTNR]_n$ (542 K), and PbTNR (596) [7], but a little lower than that of KTNP (664 K) and K_2TNR (645 K) [19, 41].

The Rb salts are more sensitive than K salts to flame, salts based on trinitrophenol are more sensitive than salts based on trinitroresorcinol to flame, and the heat sensitivities of trinitrophenol salts are lower than that of trinitroresorcinol salts.

4. Conclusion

Reaction of rubidium nitrate with the magnesium salts of trinitrophenol and trinitroresorcinol aqueous solutions gave three coordination polymers, $[RbTNP]_n$, $[Rb_2TNR{\cdot}H_2O]_n$, and $[RbHTNR]_n$. The products were characterized by elemental analysis, IR spectroscopy, and X-ray single-crystal diffraction. Thermal behaviors of the three compounds were investigated by DSC and the decomposition temperatures are higher than 473 K, meeting the requirement of stable energetic material [2]. The kinetic parameters were obtained by non-isothermal reaction kinetics, and the Arrhenius equations of $[RbTNP]_n$, $[Rb_2TNR{\cdot}H_2O]_n$,

and $[RbHTNR]_n$ can be expressed as $\ln k = 25.65–315.5 \times 10^3/RT$, $\ln k = 21.06–226.0 \times 10^3/RT$, and $\ln k = 12.10–139.3 \times 10^3/RT$, respectively. Thermal parameters of T_{p0}, T_{bp}, $\Delta S^{\neq}$, $\Delta H^{\neq}$, and $\Delta G^{\neq}$ were also obtained. Sensitivities of the compounds to heat, flame, impact, and friction were tested. The 50% firing threshold toward flame of $[RbTNP]_n$ is 50 cm and the 5 s delay explosion temperature of $[RbTNP]_n$ is 641 K. Herein, $[RbTNP]_n$ was suggested as a heat-resistant, flame sensitive eco-friendly initiator composition with a great application prospect.

Supplementary material

CCDC 979638, 979639, and 979640 contain the supplementary crystallographic data of $[RbTNP]_n$, $[Rb_2TNR{\cdot}H_2O]_n$, and $[RbHTNR]_n$, respectively. These data can also be obtained free of charge from the Cambridge Crystallographic Data Center via http://www.ccdc.cam.ac.uk/data_request/cif.

Acknowledgements

This work was supported by the National Basic Research Program of China, the Natural Science Foundation of Chongqing (cstc2011jjA50013) and the Doctoral Candidate Innovation Research Support Program by Science & Technology Review (kjdb201001-2).

References

[1] T.M. Klapötke, C.M. Sabate, J. Stierstorfer. *N. J. Chem.*, **33**, 136 (2009).
[2] M.H.V. Huynh, M.A. Hiskey, T.J. Meyer, M. Wetzler. *Proc. Natl. Acad. Sci. USA*, **103**, 5409 (2006).
[3] M.H.V. Huynh, M.D. Coburn, T.J. Meyer, M. Wetzler. *Proc. Natl. Acad. Sci. USA*, **103**, 10322 (2006).
[4] N. Orbovic, C.L. Codoceo. *Propellants, Explos. Pyrotech.*, **33**, 459 (2008).
[5] V.N. Borzdun, N.N. Dvorovenko, S.M. Ryabykh. *High Energy Chem.*, **36**, 438 (2002).
[6] M.B. Talawar, A.P. Agrawal, M. Anniyappan, D.S. Wani, M.K. Bansode, G.M. Gore. *J. Hazard. Mater.*, **137**, 1074 (2006).
[7] Z.M. Li, M.R. Zhou, T.L. Zhang, J.G. Zhang, L. Yang, Z.N. Zhou. *J. Mater. Chem. A*, **1**, 12710 (2013).
[8] X.B. Zhang, Y.H. Ren, W. Li, F.Q. Zhao, J.H. Yi, B.Z. Wang, J.R. Song. *J. Coord. Chem.*, **66**, 2051 (2013).
[9] Q. Yang, S. Chen, G. Xie, S. Gao. *J. Coord. Chem.*, **65**, 2584 (2012).
[10] B.D. Wu, Y.G. Bi, Z.N. Zhou, L. Yang, J.G. Zhang, T.L. Zhang. *J. Coord. Chem.*, **66**, 3014 (2013).
[11] Z.M. Li, T.L. Zhang, G.T. Zhang, Z.N. Zhou, L. Yang, J.G. Zhang, K.B. Yu. *J. Coord. Chem.*, **66**, 1276 (2013).
[12] F. He, K.Z. Xu, H. Zhang, Q.Q. Qiu, J.R. Song, F.Q. Zhao. *J. Coord. Chem.*, **66**, 845 (2013).
[13] G. Fan, Y.L. Zhang, J.J. Sun, M.Y. Zheng. *J. Coord. Chem.*, **64**, 3711 (2011).
[14] Z. Gao, J. Huang, K.Z. Xu, W.T. Zhang, J.R. Song, F.Q. Zhao. *J. Coord. Chem.*, **66**, 3572 (2013).
[15] A. Kovalev, H. Sturm. *Cryst. Growth Des.*, **12**, 3557 (2012).
[16] R. Liu, T.L. Zhang, L. Yang, Z.N. Zhou, X.C. Hu. *Cent. Eur. J. Chem.*, **11**, 774 (2013).
[17] Y.X. Sun, Z.L. Ren, W.S. Meng. *Asian J. Chem.*, **25**, 6186 (2013).
[18] H.T. Feng, Y.S. Zheng. *Chem. Eur. J.*, **20**, 195 (2014).
[19] D.L. Sheng, F.E. Ma. *Chin. J. Energ. Mater.*, **12**, 93 (2004).
[20] Y. Cui, T.L. Zhang, J.G. Zhang, X.C. Hu, J. Zhang, H.S. Huang. *Chin. J. Chem.*, **26**, 426 (2008).
[21] R.Z. Hu, S.P. Chen, S.L. Gao, F.Q. Zhao, Y. Luo, H.X. Gao, Q.Z. Shi, H.A. Zhao, P. Yao, J. Li. *J. Hazard. Mater.*, **117**, 103 (2005).
[22] H. Chen, T. Zhang, J. Zhang, X. Qiao, K. Yu. *J. Hazard. Mater.*, **129**, 31 (2006).
[23] H.Y. Chen, T.L. Zhang, J.G. Zhang, C.C. Chen. *Propellants, Explos. Pyrotech.*, **31**, 285 (2006).
[24] B. Shao, T.L. Zhang, J.G. Zhang, Y.M. Yang, L. Yang, K.B. Yu. *Chin. J. Energ. Mater.*, **9**, 122 (2001).
[25] Y.F. Li, T.L. Zhang, J.G. Zhang, G.X. Ma, J.C. Song, K.B. Yu. *Acta Chim. Sin.*, **61**, 1020 (2003).

[26] Y.F. Li, T.L. Zhang, J.G. Zhang, G.X. Ma, J.C. Song, Y.H. Sun, K.B. Yu. *Chin. J. Inorg. Chem.*, **19**, 861 (2003).
[27] H.Y. Chen, T.L. Zhang, J.G. Zhang, L. Yang, X.J. Qiao. *Chin. J. Chem.*, **25**, 59 (2007).
[28] L. Wang, H. Chen, T. Zhang, J. Zhang, L. Yang. *J. Hazard. Mater.*, **147**, 576 (2007).
[29] H.Y. Chen, T.L. Zhang, X.J. Qiao, L. Yang, J.G. Zhang, K.B. Yu. *Chin. J. Inorg. Chem.*, **22**, 1852 (2006).
[30] T.M. Klapötke, C.M. Sabate, M. Rasp. *Dalton Trans.*, 1825 (2009).
[31] T.M. Klapötke, C.M. Sabate, J.M. Welch. *Dalton Trans.*, 6372 (2008).
[32] J.N. Luo, K.Z. Xu, M. Wang, J.R. Song, X.L. Ren, Y.S. Chen, F.Q. Zhao. *Bull. Korean Chem. Soc.*, **31**, 2867 (2010).
[33] G.M. Sheldrick, *Acta Crystallogr., Sect. A: Found. Crystallogr.*, **64**, 112 (2008).
[34] G.M. Sheldrick, *SHELXS-97, Program for the Solution of Crystal Structure*, University of Gottingen, Germany (1997).
[35] G.M. Sheldrick, *SHELXL-97, Program for the Solution of Crystal Structure*, University of Gottingen, Germany (1997).
[36] A. Schouten, J.A. Kanters, N.S. Poonia. *Acta Cryst.*, **C46**, 61 (1990).
[37] J.G. Zhang, K. Wang, Z.M. Li, H. Zheng, T.L. Zhang, L. Yang. *Main Group Chem.*, **10**, 205 (2011).
[38] Z.M. Li, T.L. Zhang. Synthesis, crystal structure and thermal behavior of CsHTNR. Unpublished data, CCDC: 979641, (2013).
[39] H.E. Kissinger. *Analyt. Chem.*, **19**, 1702 (1957).
[40] T. Ozawa. *Bull. Chem. Soc. Jpn*, **38**, 1881 (1965).
[41] X.M. Zhang, G. Wan, T.L. Zhang, Z.M. Li, L. Yang, J.G. Zhang, Z.N. Zhou. *Chin. J. Explos. Propellants*, **35**, 61 (2012).
[42] R.Z. Hu, Z.Q. Yang, Y.J. Liang. *Thermochim. Acta*, **123**, 135 (1988).
[43] T.L. Zhang, R.Z. Hu, Y. Xue, F.P. Li. *Thermochim. Acta*, **244**, 171 (1994).
[44] J.H. Yi, F.Q. Zhao, W.L. Hong, S.Y. Xu, R.Z. Hu, Z.Q. Chen, L.Y. Zhang. *J. Hazard. Mater.*, **176**, 257 (2010).
[45] J.H. Yi, F.Q. Zhao, B.Z. Wang, Q. Liu, C. Zhou, R.Z. Hu, Y.H. Ren, S.Y. Xu, K.Z. Xu, X.N. Ren. *J. Hazard. Mater.*, **181**, 432 (2010).